Proceedings of the ASME 2010 3rd Joint US-European Fluids Engineering Summer Meeting and 8th International Conference on Nanochannels, Microchannels, and Minichannels
FEDSM-ICNMM2010
August 1-5, 2010, Montreal, Canada

FEDSM-ICNMM2010-30719

EXPERIMENTAL INVESTIGATIONS OF TRANSFER PHENOMENA IN A CONFINED PLANE TURBULENT IMPINGING WATER JET

Amine KOCHED [1]
Amine.Koched@mines-nantes.fr

Michel PAVAGEAU [1]
Michel.Pavageau@mines-nantes.fr

Fethi ALOUI [1,2]
Fethi.Aloui@univ-nantes.fr
Fethi.Aloui@mines-nantes.fr

[1] Ecole des Mines de Nantes
Département Systèmes Energétiques et Environnement (DSEE)
GEPEA CNRS UMR 6144
4 rue Alfred Kastler BP20722 44307 Nantes, France

[2] Université de Nantes
Faculté des Sciences et des Techniques Département de Physique
2, rue de la Houssiniere BP92208
44322 Nantes, France

ABSTRACT

In this study, we are interested in the hydrodynamics of impinging plane jets. Plane jets are widely used in ambience separation in HVAC, fire safety, food process engineering, cooling of electronic components etc. Despite their important industrial applications, plane jets have not been studied as extensively as axisymmetric jets. Plane jet exhibit different kind of instabilities stemming from either streamlines with strong curvature in the impingement region or inflection points in the transverse profile of the streamwise component velocity in the lateral mixing layers. Previous works in the GEPEA laboratory were performed on these flows. These works and the majority of the studies reported in the literature deal with turbulent air jets in various configurations. Very little studies have been done on water impinging jets. Taking into account the fact that the viscosity of water is smaller than air, at the same Reynolds number, it is easier to detect phenomena such as vortices. Phenomena can be observed at lower velocities making it possible to record signals with standard frequency bandwidths. This makes it easier also to do a Lagrangian tracking of vortices. We specially focused our study on the impinging zone of the jet. The dynamics of the impinging zone has not formed the subject of numerous studies. There were no studies that characterize the vortices at the impinging region of water jets in terms of size, center positions, vortex intensity, eccentricity, statistical distribution and interaction with the impinging wall. Consequently, a confined water plane jet impinging a flat plate was studied using PIV (Particle Image Velocimetry). We used POD decomposition for filtering PIV data. Then, we applied the λ_2 criterion to the recorded velocity fields to detect and characterize the vortices at the impingement. A statistical analysis was then performed. A wide range of Reynolds numbers is considered: 3000, 6000, 11000 and 16000. The corresponding results will be presented.

1. INTRODUCTION

Jet flows occur in many practical situations and are of great interest in many processes as well as in engineering applications. They are widely used for ambience separation in HVAC, fire safety [1], in food industry and in cooling of electronic components, etc. Despite their wide range of applications, planar jets have not been studied as extensively as axisymmetric jets. Only a few authors have put forward this configuration and examined it in detail; Beltaos and Rajaratnam [2], Gutmark et al. [3] and Namer and Ötügen [4]. Planar jets exhibit different kind of instabilities. These instabilities originate either from streamlines with strong curvature in the impingement region or due to inflection in the transverse profile of the streamwise velocity component in the lateral mixing layers. Taking into account those instabilities, vortices may occur. Our work has led to the identification of these flow structures in the impingement region. Previous works on impinging air jets were performed at the GEPEA laboratory (Maurel [5], Beaubert [6], Gupta [7], Abide [8], Pavageau and Loubière [9]). These works show the presence of vortices in the impingement region and their consequence on transport phenomena between the jet and the ambiance. Large Eddy Simulations (LES) [10] have shown that it is in the impingement region that mass transfer across the jet stream preferentially occurs. A lot of studies deal with heat exchange at the impingement of jets. Gardon and Akfirat [11] studied this region in terms of heat transfer between the impinging jet and the impingement plate. Suetra et al. [12,13] explained the increase in heat transfer in the impinging region by the presence of vortices. Yokobori et al. [14] showed experimentally, using visualization, roll vortices appearing in pairs of counter rotating rolls with their axis perpendicular to the plane of the jet. These rolls were associated to the Göertler vortices. Tsubokura et al. [15] observed, using LES and Direct Numerical Simulation (DNS), that the twin vortices in the stagnation region are strongly related to the counter-rotating streamwise vortices observed in the braid region for Re number lower than 6000. For high Reynolds numbers the correlation is no more proved. It has been also shown that they were characterized locally by a strong vortical intensity and noticeable energy content (Loubière and Pavageau [16]). From the foregoing discussion it is clear that, there were no studies which focused on the characterization of these vortices in terms of size, center positions, vortex intensity, eccentricity and statistical distribution except the work of Pavageau and Loubière [9] for planar air jets. It is necessary to better understand the fashion in which the large-scale structures present in the impingement region of a jet form, evolve and contribute to transfer mechanisms. The aim of our work is to detect and characterize the Göertler vortices. Further, the major studies reported in the literature deal with turbulent air jets. Planar water jets have received scant attention. Taking into account that the kinematic viscosity of water is smaller than that of air, at the same Reynolds number, it is easier to detect phenomena such as vortices. Phenomena can be observed at lower velocities making it possible to record signals with standard frequency bandwidths. Hence, it was thought desirable to undertake a systematic experimental study for confined planar submerged water slot jet impinging on a flat plate. PIV measurements have been performed in water for four different Reynolds numbers: 3000, 6000, 11000 and 16000. In order to detect vortices near the impingement, the instantaneous flow fields for different measurement planes were post-processed first by employing POD decomposition. The analysis of the most energetic POD modes shows some specific zones with high level of energy. Later, the λ_2 criterion (Jeong and Hussain, [17]) has been applied to expose vortices from the flow. They are then characterized in terms of size, shape, intensity, etc. Further, statistical analysis was also performed for all the recorded data. The results are presented.

NOMENCLATURE

$a(t)$	: Temporal coefficient
b	: Semi width of the nozzle (mm)
d_i	: Distance (mm)
e	: Nozzle width (mm)
f	: Frequency (Hz)
H	: Height of the jet (mm)
h_i	: Thickness of the impinging zone (mm)
I_u, I_v	: Turbulent intensity (%)
L	: Nozzle length (mm)
L_c	: Potential core length (mm)
M	: Number of spatial modes
Re	: Reynolds number
u,v	: Velocity components (m/s)
V_{max}	: Maximal velocity (m/s)
u', v'	: Fluctuating velocity component (m/s)
x,y	: Cartesian coordinates (mm)
Greek letters	
Φ	: Spatial function or POD mode (m)
λ_2	: Criteria for vortex detection (s^{-2})
λ_G	: Distance between vortices (mm)
ν	: Kinetic viscosity (m²/s)
Superscripts	
---	: Temporal average
'	: Fluctuation
Subscripts	
max	: Maximum

2. EXPERIMENTAL FACILITY

2.1. SPECIFICATIONS

A schematic diagram of the experimental facility is shown in Fig. 1. It consists of a rectangular tank with submerged rectangular slot nozzle at the bottom having the width e equal to 20 mm. The water pumped from another tank and discharged through this nozzle forms a planar jet flowing upward.

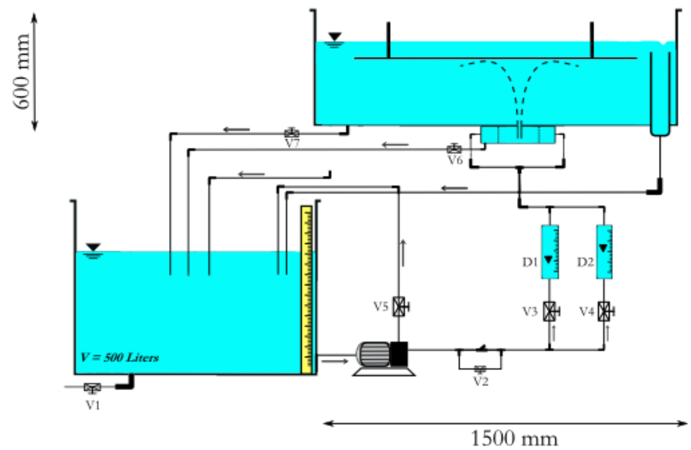

Fig. 1: Experimental setup

The jet impinges vertically on a flat plate fixed at a distance H = 200 mm from the nozzle (Fig. 2). The idea behind this is to set the geometrical aspect ratio (i.e. ratio of the height H of the jet and the nozzle width e) equal to $H/e = 10$, which is in consistence with the earlier work reported from our laboratory. Further, at this ratio, turbulent intensity at the jet axis is maximal comparing to other ratios (Gupta, [7]). The ratio for the span of nozzle L = 400 mm to the width of the nozzle e was set to $L/e = 20$ to preserve the bidimensionality of the flow.

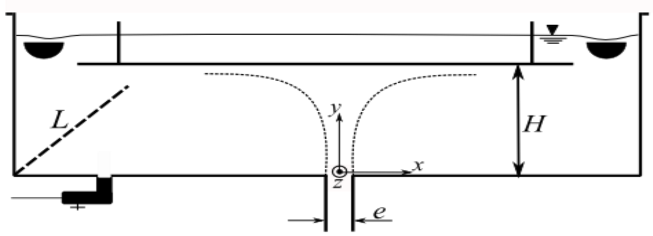

Fig. 2: Characteristic distances of the jet

The experiments were performed for four different Reynolds numbers: 3000, 6000, 11000 and 16000. The Reynolds numbers $\mathrm{Re}_{nozzle} = V_{\max} e/\nu$ were calculated using the exit velocities (V_{max}) at the nozzle, width of nozzle (e) and kinetic viscosity of water (ν). The range of the Reynolds numbers has been chosen consistently with the works of Gupta [7] and Yokobori et al. [14]. They mentioned that the Reynolds number strongly influences the mean and fluctuating characteristics of the jet when it is less than 6000. So, the Reynolds number considered cover three situations: under limit value Re = 3000, the limit value Re= 6000 and values greater than limit Re = 11000 and Re = 16000 which correspond to flowrates of 5, 10, 15 and 20m^3/h. The corresponding velocities at the nozzle exit are 0.2, 0.3, 0.55 and 0.8 m/s.

2.2. PIV MEASUREMENTS

The PIV experiments were performed using a *LaVision* acquisition system for five different planes parallel to the jet as shown in Fig. 3:

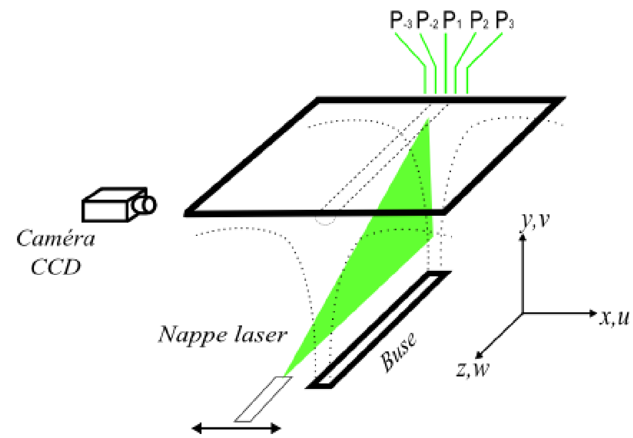

Fig. 3: Measurement planes considered for PIV technique

The positions of planes were set according to the structure of the jet (Fig. 4):

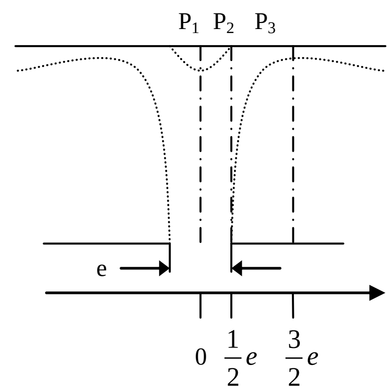

Fig. 4: Position of the planes considered for PIV measurements

The laser source adopted was a double pulsed Nd-Yag laser that had a power of 125 mJ/pulse and produces laser beam of 532 nm wavelength. It was synchronized with the camera using a synchronizer. The laser excites polyamide tracer particles (diameter equal to 20µm) in the flow. A multiframe camera, with CCD sensor resolution of 1600×1200 pixels divided into small interrogations areas of 16×16 pixels, detects the light reflected by particles at two consecutives positions and instants. An adaptative algorithm based on spatial cross-correlation technique permits to calculate the velocity vector field associated to the displacement of the different particles in the field of view. To increase the number of vectors, we use overlapping areas (mostly 50%) in the two directions. The acquisition frequency of the camera is set to 15 Hz. The time duration of recorded flow is 60 seconds. Thus, the standard PIV provides a quantity of information sufficient enough to make possible the educing of large coherent eddy structures even though a two-dimensional description of the flow field and a poor temporal resolution cannot supply all the characteristics of basically three-dimensional coherent structures.

3. FLOW CHARACTERIZATION

Many authors reported interesting phenomena about the influence of Reynolds number on the development of the jet: expansion and velocity fluctuations. Tailland et al. [18] have shown that for a range between 8500 and 38000, Reynolds number was not affecting the development of the jet. However, Namer and Ötügen [19] have shown that the expansion rate of the jet is mainly affected by the Reynolds numbers between 1000 and 7000 and they proposed a limit value for the Reynolds number which was 6000. The same limit was also proposed by Maurel [5], in study of planar air impinging jet with the important findings, that the influence of the Reynolds number still important in velocity fluctuations for $\mathrm{Re} \geq 7000$. So, before presenting results, the boundary condition at the nozzle should be defined regarding the influence of the nozzle exit velocity profile on the flow development of the jet.

3.1. BOUNDARY CONDITIONS AT THE NOZZLE

Figure 5 below shows the velocity component (longitudinal and transverse) profiles at the nozzle exit for the different Reynolds number considered here. The same figure shows flat velocity profiles, which confirms that the flow is turbulent for all Reynolds numbers. Same observations were reported by Hussain and Clark [20]. From Fig. 5 we notice that the profiles of mean longitudinal velocities are not affected by the variation of Reynolds number, unlike turbulent intensities and Reynolds tensor i.e. $\overline{u'^2}$ and $\overline{v'^2}$ (Figs.6a and 6b). The Figs. 6 shows the important turbulent activities near the boundary of the nozzle. It shows the starting of the mixing layers near the shear zone of the jet. The maximum of I_v reaches 15% for Re=16000 and 2% for Re=3000, however, the maximum of I_u didn't exceed 6%. For more details about the impinging water jet flow structure considered in this paper, readers are kindly forwarded to [21]. We will mainly focus on the impinging zone of the jet. In fact, the kinematic description of the impact region of the jet has not been the subject of many studies although significant transfers occur only in this region. The quantification and optimization of these transfers go through the understanding of mechanisms at their origin. Some works in thermal heat exchange shows a link between the increase of heat transfer activity at the impingement and Göertler vortex eddy structures formed at the impact of the jet [14,15].

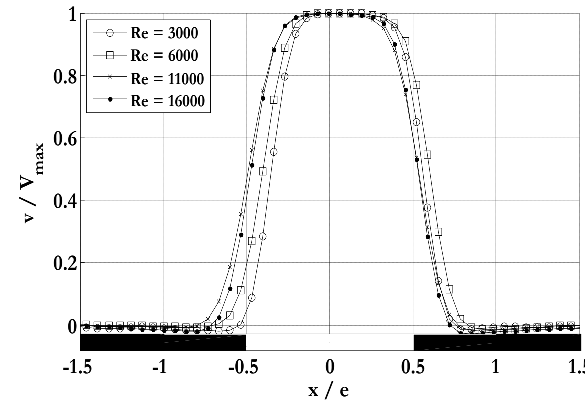

Fig. 5: Velocity profiles of the longitudinal velocity component at the nozzle

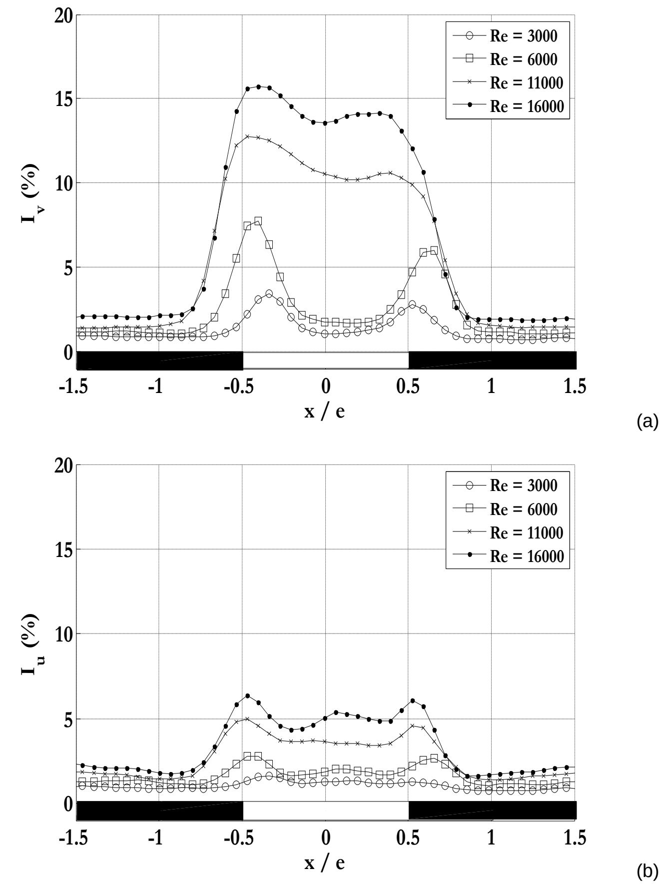

Fig. 6: Turbulent intensities at the nozzle (a) I_u (b) I_v

We will especially focus in this region on these structures in the following. We will try to understand how they evolve through the analysis of different planes parallel to the center plane of the jet as shown in Fig. 3. First, we propose to delimit this region, then we will present the technique considered for vortex detection.

3.2. THE IMPACT ZONE OF THE JET

Figure 7 shows the streamlines for the velocity field measured in the transverse plane of the jet. It shows mainly three different regions in the jet whatever the Reynolds number considered. The first region was observed nearly at $y/e = 3$ [21] from the nozzle in the direction of mean flow, the second region where the jet starts expanding and the third region is the impingement region from where the streamlines have a strong curvature, change directions and become tighten.

T ir m ai

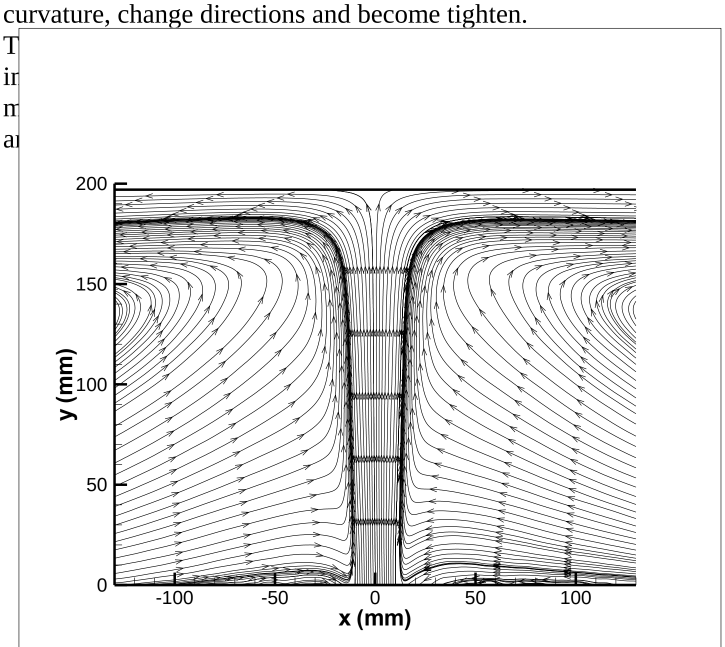

Fig. 7: Streamlines at the transverse plane of the jet (Re = 16000)

3.2.1.THICKNESS OF THE IMPACT ZONE

Gutmark et al. [3], first, estimated the thickness of the impact zone (h_i) for the planar air jet, which was about 15% of the total height of the jet (H).

In the present work the thickness of the impact zone is determined from the longitudinal profiles of Reynolds stress $\overline{u'v'}$ at three different transverse (x=b, 2b and 3b) positions with different Reynolds numbers (Fig. 8). The changing in sign of Reynolds stress values for (from + to –) reflects the starting of impact region. From Figs. 8, it has been also observed that h_i slightly affected by the Reynolds number. Indeed, for Re=3000, the ratio $h_i / H = 10\%$ and it increases only to 13% for Re=16000 (Figs. 8). Pavageau and Gupta [7], and Maurel and Solliec [22] and Pavageau et al. [24] didn't mention any influence of the Reynolds number in the case of twin and simple planar air jet and reported a ratio of $h_i / H = 13\%$.

For the characterization of vortices occurring at the impingement, we will consider an impingement region size larger than the calculated thickness of the impingement. The height of the bandwidth considered is equal to 20% of the total jet height H as we don't know how the vortices evolve far from the center plane of the jet.

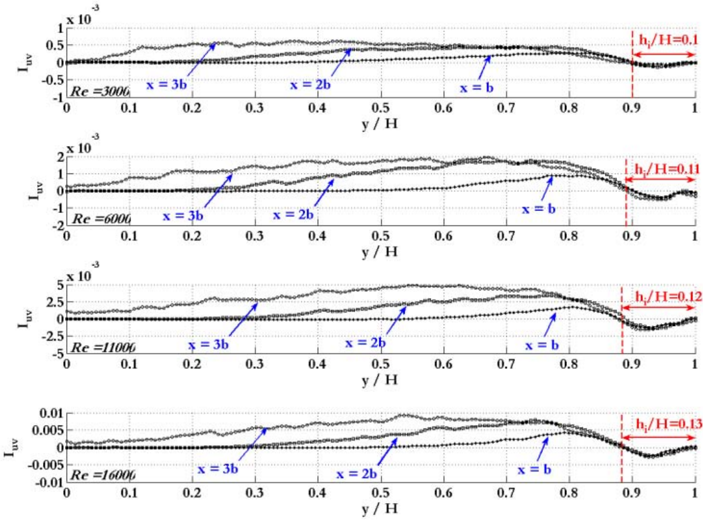

Fig. 8: Variation of $\overline{u'v'}/V_{max}^{2}$ with Re number; H/e = 10

3.2.2.VORTEX AT THE IMPINGEMENT OF THE JET

A. DETECTION METHOD

PIV measurements give the global flow field of the jet. They also efficiently provide information about the associated eddy structures in the near-wall or impact region. Hence, it is quite possible to point out the influence of the impingement on the longitudinal and transverse mean flow. Four different Reynolds numbers were considered in order to study their influence on the size of the eddy structures at the impingement region. Yokobori et al. [14] and Sakakibara et al. [24] underlined the presence of Göertler counter rotating structures in the impinging zone. They specified that these structures were due to the fact that the impingement was at the level of the transition zone of a free jet. Thus, they concluded without any strong argument that these structures disappear when $H/e > 15 \approx 20$. To detect vortices at the impingement, we considered PIV measurements on different planes of the jet. First, we considered a parallel plane to the impinging plate (Fig. 9), and then we considered different planes parallel to the center plane of the jet (Fig. 3):

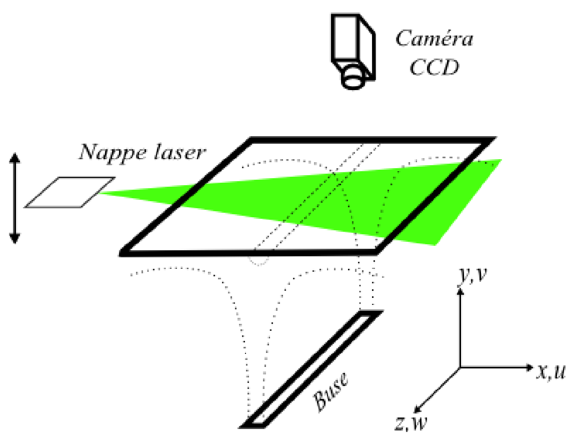

Fig. 9: PIV measurement in a plane parallel to the impingement

Due to the diversity and complexity of flows where these coherent structures are embedded, no consensual and general definition of such structures is yet established. Nevertheless, it is agreed that they refer to large-scale organized swirling motions and that, during their transport, they should exhibit a certain degree of integrity over certain spatial and temporal scales. Their separation from background turbulence doesn't rely on one unique method.

Structure identification requires the computation of spatial derivatives of the fluid velocity. A certain smoothness of the velocity field under study must be ensured. However, PIV measurements are discrete in space, with a relative spatial resolution usually much below than the numerical one. They additionally contain a certain level of noise which must be filtered. In the present work, a method of filtering based on proper orthogonal decomposition (POD) technique (Lumley et al. [25]) was first applied to the instantaneous velocity fields. Filtering consists in removing from the fluctuating velocity fields the effects of perturbation on the flow (mainly due to laser reflexion, particle deposition, etc.).

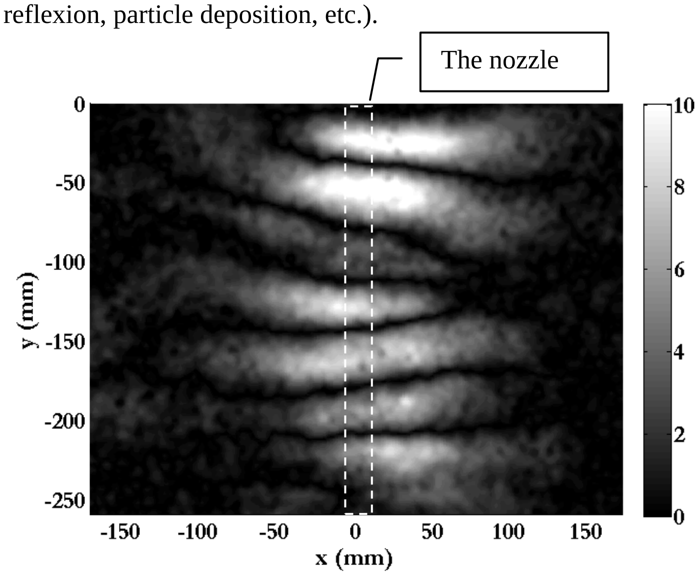

Fig. 10: 11th spatial mode (Φ_{11})

So, the dominant topology will be extracted using spatial functions $\Phi^{(k)}(r)$ and temporal coefficient $a^{(k)}(t)$:

$$u(r,t) \cong \overline{u(r,t)} + \sum_{k=1}^{M} a^{(k)}(t).\Phi^{(k)}(r) \qquad (1)$$

The analysis of the spatial mode (11th mode) issued from PIV measurements according to configuration shown in Fig. 8, shows an elongated transverse energetic activity at the impingement. It is possible that this activity is due to Göertler vortices evolving at the impingement of the jet (Fig 10).

The analysis of different spatial modes associated to PIV measurement configuration shown in Fig. 3 shows also a similar activity near the impingement (Fig11).

Here, authors would like to put the emphasis on the high energy zones detected at the developed region of the jet (50 < y < 130 on Fig. 11). This energy is mainly due to Kelvin-Helmholtz vortices in the mixing layers of the jet. The analysis of spatial modes presented in Figs 10 and 11 is important to have an idea about the probable positions of vortices in the jet and near the impingement. In any way, the information given by the spatial modes could be used to characterize the vortices in terms of size, shape, vortical intensity etc. Rambaud et al. [26] have shown, through different tests on analytical and experimental vortices, that the direct analysis of spatial mode may induce to error when used to characterize vortices.

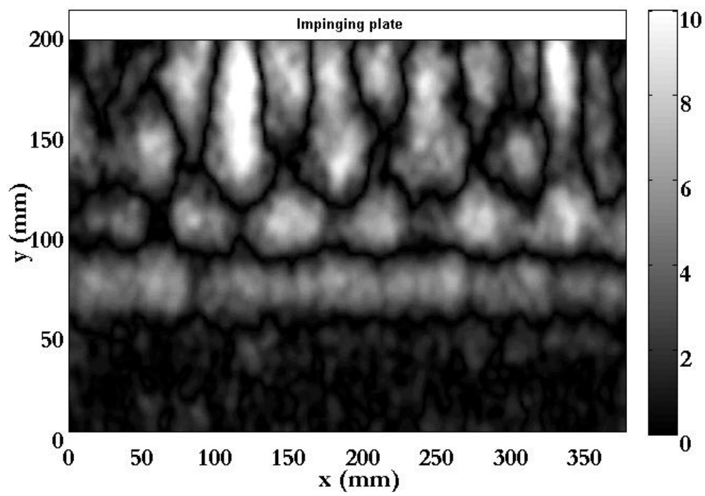

Fig. 11: 11th spatial mode (Φ_{11})

The identification method applied in this work starts with the detection of the position of vortex core center by using the so-called λ_2 criterion (Jeong and Hussain [17]). A translational velocity is then estimated for every detected vortex core and is subtracted from the total field in which the vortex has been detected, before analysis of the topological features and energy content of all detected vortices.

The λ_2 criterion has two main interesting properties for coherent structures eduction:

- To discriminate swirling and shearing motion (what is not achieved by visualizing only vorticity),
- To be frame independent (vortex identification doesn't require a choice of a reference frame to visualize the detected vortex cores).

This criterion is based on the assumption that a vortex core center is associated to the existence of a local pressure minimum. It is derived from the equation verified by the Hessian of pressure $\partial^2 P / \partial x_i x_j$. This quantity provides information about pressure extrema. The equation is obtained by applying the gradient operator on the Navier-Stokes equations (Jeong and Hussain [17], on the identification of a vortex):

$$\frac{d}{dt}\left(S_{ij}\right) - \nu \frac{\partial^2 S_{ij}}{\partial x_k \partial x_k} + \Omega_{ik}\Omega_{kj} + S_{ik}S_{kj} = -\frac{1}{\rho}\frac{\partial^2 p}{\partial x_i \partial x_j} \qquad (2)$$

where

$$S_{ij} = \frac{1}{2}\left(\frac{\partial U_i}{\partial x_j} + \frac{\partial U_j}{\partial x_i}\right) \qquad (3)$$

is the component of the symmetric deformation rate tensor S.

$$\Omega_{ij} = \frac{1}{2}\left(\frac{\partial U_i}{\partial x_j} - \frac{\partial U_j}{\partial x_i}\right) \qquad (4)$$

is the component of the antisymmetric spin tensor Ω.

Jeong and Hussain [17] attribute to the sum $\Omega_{ik}\Omega_{kj} + S_{ik}S_{kj}$ the occurrence of pressure minima due solely to coherent vortices. Denoting by $\lambda_1 \geq \lambda_2 \geq \lambda_3$, the three eigenvalues of this tensor, a variational analysis shows that pressure reaches a local minimum if and only if two of these eigenvalues are negative.

The equivalent condition $\lambda_2 < 0$ was then proposed for the definition of a vortex core. Vortices can subsequently be visualized by plotting $iso-\lambda_2$ contours. The application of λ_2 criterion on 2D vector field returns negative peaks that are not all relevant as some of them do not necessarily correspond to large values of the enstrophy field [27]. This peaks can easily be removed by applying a threshold and by retaining only the values of λ_2 such that $\lambda_2 < \lambda_{2,\,threshold}$. The difficulty lies in the choice of an appropriate value of the threshold. According to [9,16,27], the method used actually leads to removing the values of λ_2 whose absolute value is lower than 40% of the absolute value $\left|\lambda_{2,\min}\right|$ of the absolute minimum of λ_2 calculated for the current instantaneous field.

To characterize the detected vortices, we examined the distribution of the tangential component of velocity V_θ around the vortex center. It is here assumed that a vortex core is marked by an increase in tangential component of velocity with radial position inside the vortex, and by a decrease in tangential component of velocity with radial position outside the vortex. Subsequently, the size and shape of a detected structure is estimated by finding the maxima of V_θ along 8 directions as shown on Fig. 12.

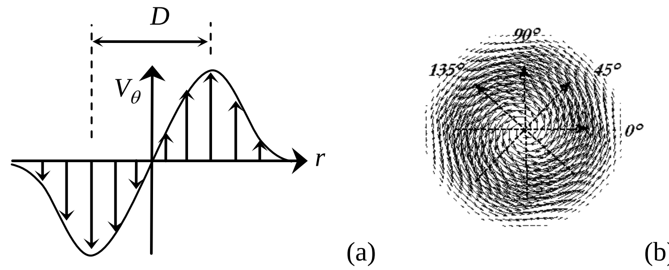

Fig. 12: (a) Tangential component velocity profile within the core of a vortex; (b) Radial directions considered for diameter estimation of the vortex

From this, it is defined for each vortex:

- A mean diameter:

$$D_m = \frac{1}{4}\sum_{\alpha=0°,45°,90°,135°} D_\alpha \qquad (5)$$

- An eccentricity:

$$E_x = \frac{\max\left(D_\alpha\right)}{\min\left(D_\alpha\right)}, \quad \alpha = 0°, 45°, 90°, 135° \qquad (6)$$

The informations below are stored for each vortex detected from all the instantaneous velocity fields:

- Number of the snapshot from which the structure was detected,
- Vortex core center coordinates,
- Diameters $D_\alpha \left(\alpha = 0°, 45°, 90°, 135° \text{ and mean diameter}\right)$
- Eccentricity,
- Rotation direction (according to the sign of vorticity at the center of the detected vortex).

The probability density functions of the detected vortices on series of instantaneous velocity field are calculated. The percentage of vortices having a counter-clockwise/clockwise rotation direction is also calculated.

B. RESULTS OF STATISTICAL ANALYSIS

As mentioned before in the §2.2.1, the size of the region in the impingement zone where statistical analysis is made, is $h \times L = 0.02H \times L$. So, results presented in this section are for the considered region and not for all of the jet.

The total number of vortices detected for the different Reynolds numbers and in the different planes considered (as mentioned in Fig. 3) is summarised in the figure below:

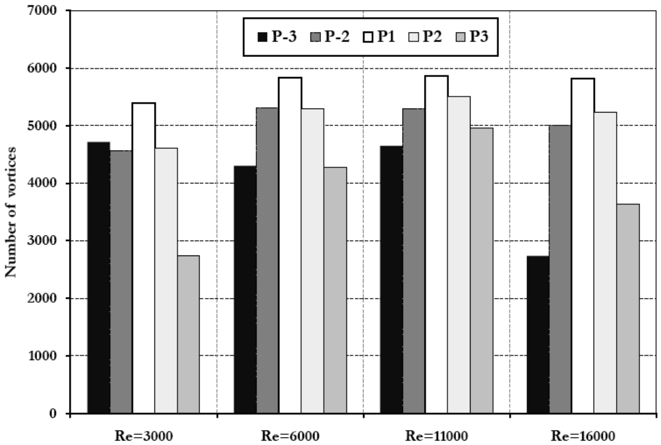

Fig. 13: Number of vortex detected for each plane and Reynolds number considered

According to Fig. 13, it is shown that for $\mathrm{Re} \leq 6000$, the number of vortices in the left side of the jet (planes P_{-2} and P_{-3}) is larger than the number of vortices in the right side of the jet. This tendency is inversed for $\mathrm{Re} \geq 6000$. The Reynolds number has an influence on the number of vortices evolving in the different considered planes. In the planes P_1, P_2, and P_{-2}, the number of vortices increases while increasing the Reynolds number. For the planes P_3 and P_{-3}, this conclusion is no more valid.

Further, out of the total vortex detected in each planes for the different Reynolds number considered, the vortices with clockwise rotation and with anticlockwise rotation have nearly equal percentage (Fig. 14).

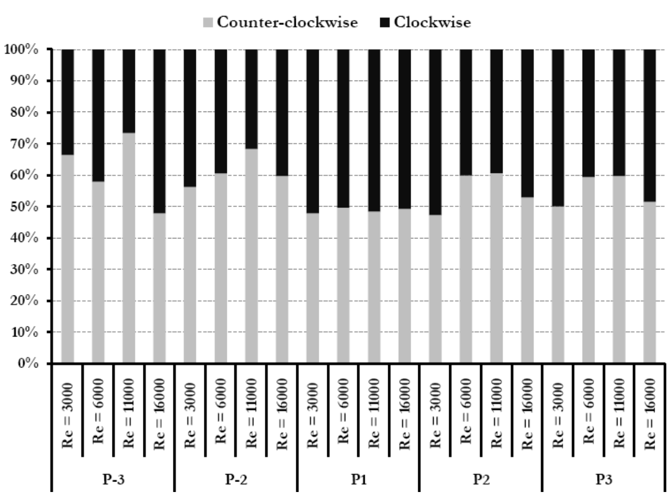

Fig. 14: Percentage of counter-clockwise and clockwise vortices

The probability density functions of the mean diameter of the detected vortices (D_m) are plotted in Fig. 15. Most of the detected structures have their mean diameter comprised between 4 and 30 mm i.e. between e/5 and 1.5e.

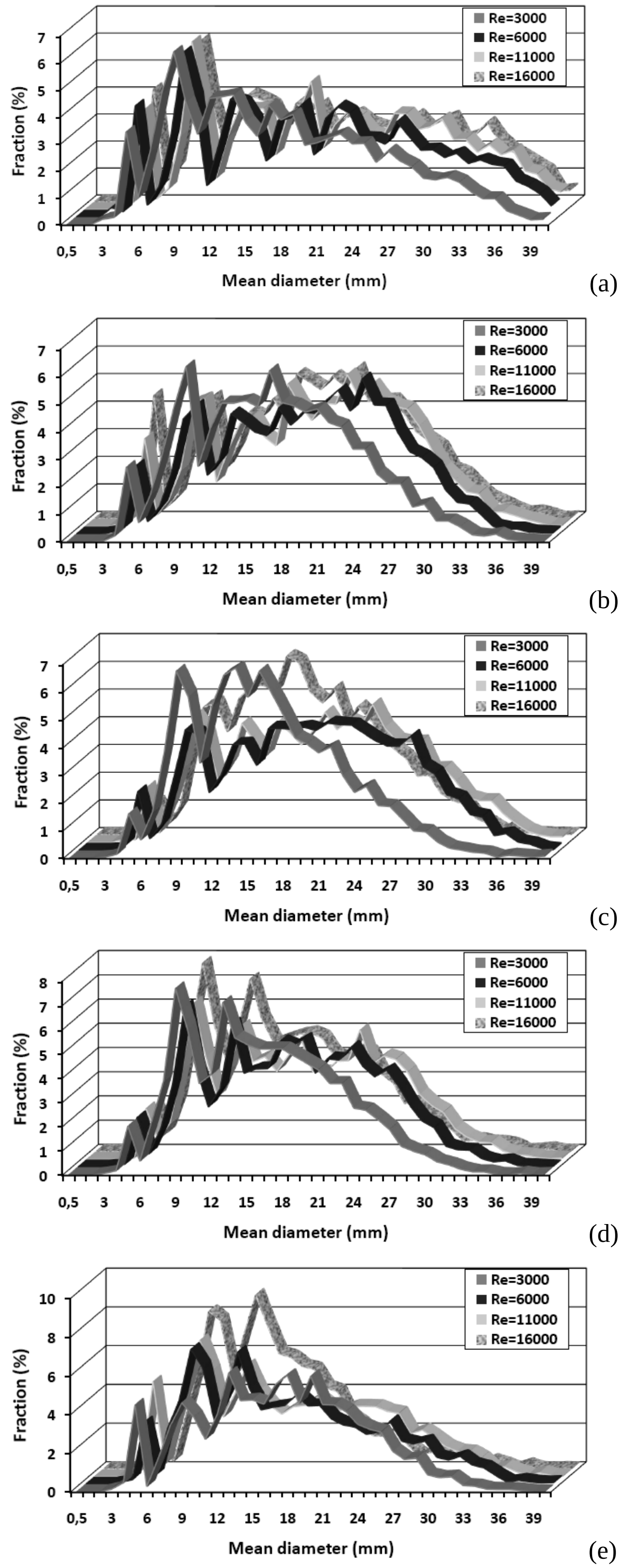

Fig. 15: Probability density function of the mean diameter of vortices in the different planes: (a) P_1; (b) P_2; (c) P_3; (d) P_{-2}; (e) P_{-3}

Fig; 15.a shows the presence of big size vortices (D_m > 30mm) vortices which is confusing according to the size h_i of the considered region for the statistical analysis. We cannot exclude the limit of the technique for characterization of vortices evolving from this plane. It is better to consider for such study, planes far from the center of the jet such as planes P_2 or P_{-2}.

The probability density function of eccentricity doesn't varies significantly for the different planes and for considered Reynolds numbers. A sample of the obtained results is shown on Fig. 16 for the case of eccentricity calculated for vortices detected on the plane P_2. Most of the vortices are characterized by an eccentricity range between 1.2 and 3.6. All these findings prove that the shape of the detected vortices is elliptical.

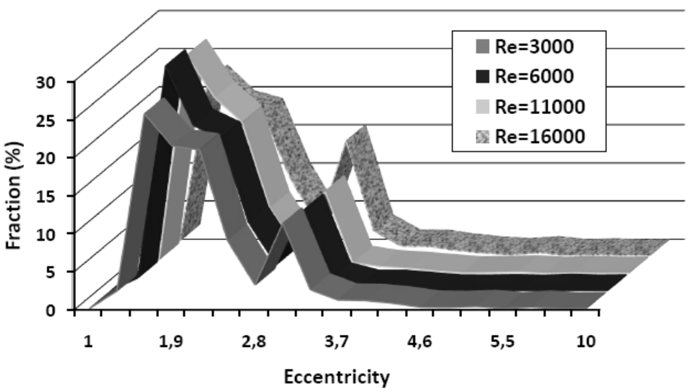

Fig. 16: Probability density function of eccentricity of vortices (plane P_1 at the center of the jet)

4. CONCLUSIONS

The present paper focuses on the development of planar vertical impinging water jet and the flow structure in the impingement region of such flow. The study was directed towards the impinging region. A characteristic height of this area h_i was calculated and it is found between 10% and 13% of the total height H of the jet. Then, we focus on the vortex structure evolving in the impingement of the jet. A vortex educing method developed in our laboratory was used to better understand the fashion in which the large-scale structures form, evolve and contribute to transfer mechanisms. The employed algorithm is based on λ_2 criterion [17]. This criterion is used here to detect and locate the vortex core center, the topological features of a structure being inferred from a local examination of the velocity field. It was found that:

- The Reynolds number has an influence on the number of vortices evolving in the different considered planes,
- Vortex covering a wide range of sizes (from 4 mm to 30 mm) co-exists in this region,
- The fraction of vortices having clockwise rotation direction is close to the proportion of vortices having a counter clockwise rotation direction,
- The shape of the detected vortices is predominately ellipsoidal.

In the future, further work will be done to understand the role of these structures in the transfer mechanisms with the impinging plate.

ACKNOWLEDGMENTS

This research was supported by GEPEA Laboratory and the Department of Energetic and Environmental Systems at Ecole des Mines de Nantes. These supports are gratefully acknowledged.

REFERENCES

[1] Gupta, S., and Pavageau, M., 2007, “Cellular confinement of tunnel sections between two air curtains”, Building and Environment, 42(9), pp. 3352 – 3365, (2007).
[2] Beltaos, S., and Rajaratnam, N., 1973, “Plane turbulent impinging jets”, I. J. of Hydraulic Research, pp. 29-60.
[3] Gutmark, E., Wolfshtein, M., Wygnanski I., 1978, “The plane turbulent impinging jet”. J.Fluid Mech. 88(4), pp.737 - 756.
[4] Namer, I., and Ötügen, M.V., 1988, “Velocity measurements in plane turbulent air jet at moderate numbers”, Exp. Fluids, 6, pp.387-399.
[5] Maurel, S., 2001, “Etude expérimentale d’un jet plan en impact. Analyse paramétrique et caractérisation des transferts de masse”, Ph.D. thesis, University of Nantes, France.
[6] Beaubert, F., 2002, “Simulation des grandes échelles turbulentes d’un jet en impact”, Ph.D. thesis, University of Nantes, France.
[7] Gupta, S., 2005, “Etude expérimentale du comportement dynamique et des performances de rideaux d’air en vue de la conception de systèmes de confinement cellulaire”, Ph.D. thesis, University of Nantes, France.
[8] Abide, S., 2005, “Une méthode de décomposition de domaine pour la simulation numérique directe Contribution à l’étude de jets plans en impacts”, Ph.D. thesis, University of Nantes, France.
[9] Pavageau, M., and Loubière, K., 2006, “Automatic eduction and statistical analysis of coherent structures in the wall region of a confined plane turbulent impinging jet”, Experiments in Fluids, pp.35-55.
[10] Beaubert, F., and Viazzo, S., 2001, “Etude d’un jet plan turbulent en impact proche par simulation des grandes échelles”, Proc. SFT: Transferts de chaleur et de masse dans les jets, Paris, France
[11] Gardon, R., Akfirat, J.C., 1965, “The role of turbulence in determining the heat transfer characteristics of impinging jets”, Int. J. Heat Mass Transfer, 12, pp.1261-1272.

[12] Suetra, S.P., Maeder, P.F., Kestin, J., 1963, “On the sensitivity of heat transfer in the stagnation-point boundary

layer to free-stream vorticity", J. Fluid Mech., 16, pp.497-520.
[13] Suetra, S.P., 1965, "Vorticity amplification in stagnation-point flow and its effect on heat transfer", J. Fluid Mech. 21(3), pp.513-534.
[14] Yokobori, S., Kasagi, N., Hirata, M., 1983, "Transport phenomena at the stagnation region of a two-dimensional impinging jet", Trans. JSME ser. B 49(441), pp.1029-1039.
[15] Tsubokura, M., Kobayashi, T., Taniguchi, N., Jones, W.P., 2003, "A numerical study on the eddy structures of impinging jets excited at the inlet", Int. J. of Heat and Fluid Flow, pp.500-511.
[16] Loubière, K., Pavageau, M., 2008, "Educing coherent eddy structures in air curtains systems", Chemical engineering and Processing, 47, pp.435-448.
[17] Jeong, J., Hussain, F., 1995, "On the Identification of a vortex", J. Fluid Mech., 285, pp.69-94.
[18] Tailland, A., Mathieu, J., 1967, "Jet Pariétal", J.Mécanique, 6, pp.103-131.
[19] Namer, I., Ötügen, M.V., 1988, "Velocity measurements in plane turbulent air jet at moderate numbers", Exp. Fluids, 6, pp.387-399.
[20] Hussain, A.K.M.F, Clark, A.R., 1977, "Upstream influence on the near field of a plane turbulent jet", The Physics of Fluids, 20(9), pp.1416-1426.
[21] Koched, A., Pavageau, M., Aloui, F., 2010, "Vortex struture in the wall region of an impinging plane jet", Proc. 2nd International conference on energy conversion and conservation, CICME10, April, 22-25.
[22] Maurel, S., Solliec, C., 2001, "A turbulent plane jet impinging nearby and far from a flat plate", Experiments in Fluids, 31, pp.687-696.
[23] Maurel, S., Rey, C., Solliec, C., Pavageau, M., 2004, "Caractéristiques cinématiques et structurelles d'un jet d'air plan turbulent frappant une plaque plane placée à distance variable", Mécaniques & Industries 5, pp.317-329.
[24] Sakakibara, J., Hishida, K., Maeda, M., 1997, "Vortex structure and heat transfer in stagnation region of an impinging plat jet (simultaneous measurements of velocity and temperature fields by digital particle image Velocimetry and laser-induced fluorescence)", Int. J. Heat and Mass Transfer, 40(13), pp.3163-3176.
[25] Lumley, J. L., 1967, "The structure of inhomogeneous turbulent flows", In. A. M. Ialglom& V.I. Tatarski editors, Atmospheric Turbulence and Ratio Wave Propagation, pp.221-227.
[26] Rambaud, P., Régert, T., Riethmuller, M.L., 2006, "Décomposition Orthogonale et interprétation directe des modes propres", Proc. Congrès Francophone de Techniques Laser CFTL06, Toulouse, 19-22 Septembre (2006).
[27] Schram, C., Rambaud, P., Riethmuller, M.L., 2004, "Wavelet based eddy structure eduction from backward facing step flow investigated using PIV", Exp. Fluids, 36, pp. 233-245.

